Available online at www.sciencedirect.com
ScienceDirect
Ceramics International 37 (2011) 2467–2476
CERAMICS INTERNATIONAL
www.elsevier.com/locate/ceramint

Effects of pre-strain applied at a polyethylene terephthalate substrate before the coating of Al-doped ZnO film on film quality and optical and electrical properties

Tse-Chang Li [a], Po-Tsung Hsieh [b], Jen-Fin Lin [a,b,*]

[a] Department of Mechanical Engineering, National Cheng Kung University, Tainan 701, Taiwan
[b] Center for Micro/Nano Science and Technology, National Cheng Kung University, Tainan 701, Taiwan

Received 6 March 2011; accepted 29 March 2011
Available online 8 April 2011

Abstract

Five kinds of polyethylene-terephthalate (PET)/aluminum-doped zinc oxide (AZO) specimen were prepared to examine the effect of strain applied to the PET substrate before the coating of AZO film on the mechanical, optical, and electrical properties and morphology. An increase in the strain of PET increases the reflection intensity, resulting in a significant reduction in absorption. The largest mean surface roughness was obtained for the PET-4%/AZO specimen. XRD diffraction peaks of ZnO (002) indicate that the quality of the AZO film initially improved with increasing strain, and then degraded with further increases. Compressive residual stresses formed in the bending specimens at various strains; the residual stress increased with decreasing 2θ angle. A higher compressive stress in the AZO film resulted in a lower optical band gap and a lower transmittance; it also led to an increase in the sheet resistance of the AZO film, and thus a lower carrier mobility.

Keywords: B. Defects; E. Substrates; D. ZnO; Pre-strain

1. Introduction

The physical and mechanical properties of polymers strongly depend on molecular orientation, which can be introduced by drawing or extrusion. Such a process changes the structure of the polymer surface as well as the bulk phase. The application of Fourier transform infrared spectroscopy (FTIR) for obtaining horizontal angular profiles of infrared (IR) absorbance from several polymer surfaces was described by Yuan and Sung [1]. FTIR-ATR (attenuated total reflectance) spectra for uniaxially drawn polyethylene-terephthalate (PET) films were obtained as a function of horizontal angles. The bound at 795 cm^{-1} may be used as an indication of the overall chain orientation. In the study of Liu *et al.* [2], pure green-emitting luminescent materials, Tb^{3+}-doped ZnO nanocrystals, were synthesized. An energetic model was proposed to identify the stretching types of the four large absorption bands shown in the FTIR spectra. Van den Heuvel *et al.* [3] developed a method for measuring IR spectra during the mechanical deformation of PET yarns. This rheooptical technique was applied to study the molecular processes that took place along the stress-strain curve of PET yarns at elevated temperatures. Zinc oxide coatings have been deposited on polyethylene terephthalate to study the influence of the sputtering parameters on the properties of the coatings [4]. The composition and the optical constants, including the optical band gap of the ZnO films, varied over a wide range depending on the sputtering parameters. Treatment of the PET surface by cold plasma improves the adhesion of ZnO films. In the study of Wu *et al.* [5], single-crystal ZnO nanorods were prepared to investigate the effect of annealing ambiance on the optical properties. Nano-ZnO/PET and nano-ZnO/polyethylene glycol (PEG)/PET composites were synthesized via the in- situ polymerization of the PET in the work of Tao *et al.* [6]. The experimental results showed that nano particles can accelerate the crystallization of the PET, which was demonstrated by increased intensities of the XRD peaks.

Highly conductive and transparent (in the visible range) Al-doped ZnO (ZnO:Al) and undoped ZnO films have been deposited by radio frequency (RF) magnetron sputtering [7].

* Corresponding author. 1 University Road, Tainan 701, Taiwan (R.O.C.). Tel.: +886 6 2757575x62155; fax: +886 6 2352973.
E-mail address: jflin@mail.ncku.edu.tw (J.-F. Lin).

0272-8842/$36.00.
doi:10.1016/j.ceramint.2011.03.042

Undoped ZnO films have a texture axis parallel to the substrate. In contrast, ZnO films have a columnar texture with its axis perpendicular to the substrate. Phonon modes detected at 516 cm^{-1} and 468 cm^{-1} are well pronounced in the Raman spectra for the doped samples. In the study of Water and Chu [8], poly-crystal ZnO films with c-axis (002) orientation were grown on a Si substrate. The sputtering conditions influenced the surface roughness. Al-doped $Zn_{1-x}Mg_xO$ films were deposited on glass substrates at a substrate temperature of 200 °C [9]. Band-gap modified transparent conducting films were realized using Al-doped $Zn_{1-x}Mg_xO$. The resistivity increased with increasing band-gap energy. In the work of Hong *et al.* [10], a series of ZnO thin films were deposited on ZnO buffer layers by DC reactive magnetron sputtering. With an increase of the buffer layer thickness, the band gap edge shifted toward longer wavelengths.

High-quality transparent conductive ZnO thin films have been deposited on quartz glass substrates using pulsed laser deposition (PLD). The control of growth conditions for obtaining good-quality ZnO films was addressed in the study of Park *et al.* [11]. The influence of growth conditions on the structural properties is related to essence of films. The optical properties of wide-band-gap semiconductors are currently being intensively investigated. Makino *et al.* [12] studied the evolution of optical absorption spectra in eight samples of n-type ZnO:Al. The strong Coulomb interaction between electrons and holes inherent to ZnO may be related to the persistence of the edge singularity up to room temperature. In the study of Gupta *et al.* [13], highly transparent and conducting thin films of ZnO-In_2O_3 were deposited. The effects of composition and growth temperature on the structural, electrical, and optical properties were studied. The incorporation of indium into ZnO and high substrate temperature improved the surface roughness of the films. Al-doped ZnO thin films were prepared by PLD on a quartz substrate in the study of Vinodkumar *et al.* [14]. The presence of a high-frequency E_2 mode and longitudinal optical A_1 (LO) modes in the Raman spectra suggest a hexagonal wurtzite structure with preferred orientation along the (002) plane for the films. 1% Al-doped ZnO film exhibits high transmittance in the visible and near infrared regions and low DC electrical resistivity. Ding *et al.* [15] used the RF reactive magnetron sputtering technique to prepare Al-doped ZnO (ZnO:Al) thin films with various Al content levels. The crystallinity of the films improved when an appropriate amount of Al was added. The residual compressive stress decreased at high annealing temperatures. In the work of Kim *et al.* [16], the effects of O_2 plasma pretreatment on the properties of Ga-doped ZnO films deposited on a PET substrate were studied. With increasing O_2 plasma treatment time, the contact angle decreased and the RMS surface roughness significantly increased. The transmittance of GZO films deposited on a PET substrate at a wavelength of 550 nm was 70∼84%. In the study of Fortunato *et al.* [17], the optical, electrical, structural, and mechanical properties of aluminum-doped zinc oxide (ZnO:Al) thin films deposited on polymeric substrates were investigated. The influence of uniaxial tensile strain on the electrical resistance of the thin films was evaluated during tensile elongation. An increase in electrical resistance is related to the number of cracks, as well as the crack width, and the film thickness. Low-temperature deposition of ZnO films was conducted by Banerjee *et al.* [18] on PET substrates. The films showed a proper formation of hexagonal ZnO. The optical properties, band gap values, and room-temperature conductivities of the films were deeply affected by the substrate material. Song [19] studied the effects of RF power on the surface morphological, structural, and electrical properties of aluminum-doped ZnO films. The root-mean-square roughness almost linearly increased with increasing power; the optical band gap of the films increased with increasing power. Sierros *et al.* [20] deposited ZnO films with various thicknesses on PET and polyethylene naphthalate (PEN) flexible substrates and measured their mechanical properties. It was found that the scratch resistance of ZnO is thickness-dependent. An Al-doped ZnO conducting layer was deposited on a PET substrate to investigate the possible application of the film as a transparent conducting electrode. The structural and electrical properties of ZnO:Al thin films are influenced by the position of the PET substrate and the gas pressure [21].

In the present study, five kinds of PET/aluminum-doped zinc oxide (AZO) specimen were prepared to investigate the effect of the strain applied to the PET substrate before the coating of the AZO film on the mechanical, optical, morphological, and electrical properties. The Al-doped ZnO (ZnO:Al) films were deposited by an RF magnetron sputtering system on the PET substrates. The PET sheet was pressed against the partial-arc plate with various strains during the coating process of AZO films (ZnO: Al with 3% Al_2O_3). Before the coating of the thin film, tensile tests were carried out for the PET substrate to evaluate its yield stress, strain, and elastic modulus under various tensile speeds. FTIR spectra for the PET substrates with various strains were obtained in order to investigate their reflection and absorption performance; wavenumber (group frequency) ranges was used to identify the vibration mode. The scanning electron microscopy (SEM) morphologies are used to examine the effect of the strain in the substrate on the surface roughness after the coating of AZO films. X-ray diffraction (XRD) patterns for the PET/AZO specimens are used to identify the primary orientation of the ZnO film and the 2θ angle corresponding to their peak value, which is needed in the calculation of the thin film stress. The interplanar spacings of the PET/AZO specimens depend on their residual stress. The Raman spectra of the four specimens are provided to illustrate the effect of strain in the substrate on the residual stress, structural disorder, and crystal defects in the films. The effect of strain in the substrate on the optical transmittance and absorption and their mean values is also evaluated. The values of the absorption coefficient for various strains are obtained to determine the optical band gap. A relationship between the four-point resistance and the optical band gap is established through the investigation of carrier mobility for each specimen.

2. Experimental Details

In the present study, AZO thin films were deposited on a PET substrate using an RF magnetron sputtering system (Helix,

Table 1
Details of the deposition conditions.

Target	AZO (ZnO:Al)
Target diameter (mm)	75
Source to substrate distance (cm)	5
Substrate temperature (°C)	room temperature
Power (W)	100
Chamber pressure (Pa)	2.67
Ar flow rate (sccm)	19
O_2 flow rate (sccm)	1
Presputtering time (s)	180
Sputtering time (s)	7200

Table 2
Basic physical and mechanical properties of polyethylene terephthalate (PET).

Density (g/cm^3)	1.33
Tensile strength at yield (MPa)	57-59
Elongation at yield (%)	4
Modulus of elasticity (GPa)	2.2
Tear strength (kN/m)	54-59
Specific heat capacity (J/kg°C)	1100
Haze (%)	0.8
Ratio of transmission (%, visible)	89

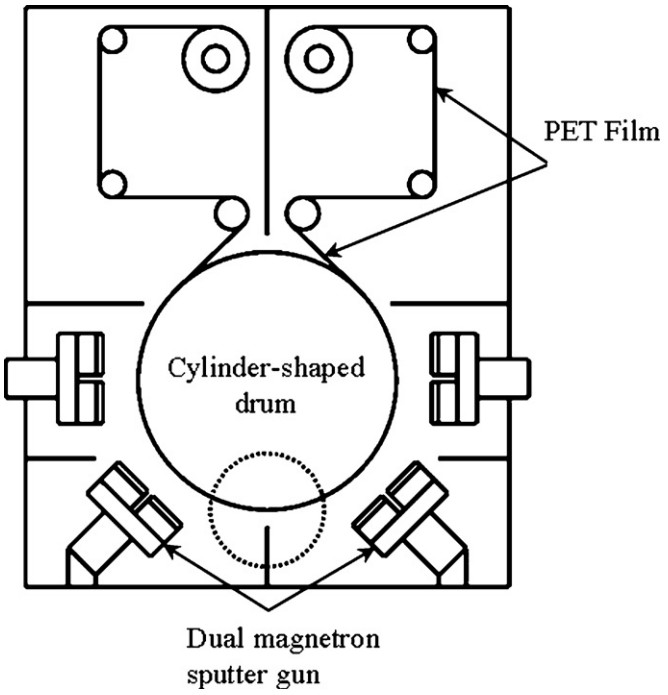

Fig. 1. Diagram of rotating deposition system.

HLLS-87, Taiwan). During the sputtering process, the AZO target had a composition of ZnO:Al with 3% Al_2O_3 and a diameter of 75 mm. The deposition conditions are shown in Table 1. The PET substrate had a thickness of 188 μm. The basic physical and mechanical properties of PET are listed in Table 2.

In the mass production of rollable and foldable electronics, a thin ceramic film coating on a soft, flexible substrate is efficiently deposited on a rotating deposition system, as shown in Fig. 1. The flexible substrate sheet is pressed against a rotating cylindrical drum, which is driven by frictional torque due to the tangential forces applied at the front and back sides of the moving PET substrate sheet belt. The ceramic film is then deposited by magnetron sputter guns when the substrate sheet has rotated to the deposition positions. In order to simulate this deposition process, the mould shown in Fig. 2(a) was designed in this study. A schematic diagram of the mould is shown in Fig. 2(b). In this rig, the rectangular plate with a partial-arc top surface is fixed at the central region of the circular flat plate by a screw. The radius of curvature of the partial-arc top surface was designed to be as same as that shown in Fig. 1, which was measured as 50 cm. A rectangular PET (SHINPEX, C87R8H, Taiwan) sheet was held at its two ends by clamps such that the sheet specimen remained fixed on the partial-arc plate. The PET specimen can be elongated to produce various strains by adjusting a screw while remaining symmetrical can be slightly elongated to produce with respect to the central line of the rectangular plate. The original length of the specimen before the tension force is applied is defined as L_0. The specimen is then elongated to a length L after the tension force is applied. The strain (ε) created in the specimen is defined as $(1–L_0/L) \times 100\%$. Four strain values, including no strain (0% strain), were selected in the present study to investigate the strain effect on the coating quality of the AZO film. The device shown in Fig. 2(a) with a PET sheet specimen was installed in the chamber of a DC magnetron sputtering system (HELIX HLLS-87, Taiwan) after a strain was applied to deposit the AZO film at a constant time of 7200s.

Tensile tests for the PET substrate material were carried out on a tester (Hung Ta HT-9600, Taiwan) following the ASTM-

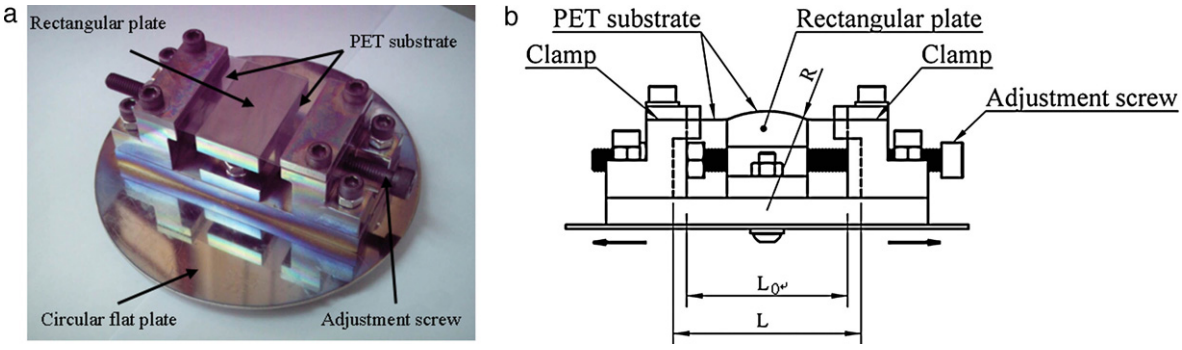

Fig. 2. (a) Photograph and (b) schematic diagram of the mould.

D638-03 method with three tensile speeds, namely 1, 10, and 50 mm/min. The span length of the specimen was 25 mm. The yielding stress and elastic modulus of the PET material were obtained as functions of the tensile speed.

The FTIR spectra, taken in the mid-IR region of 700 to about 3100 cm^{-1}, for the PET substrates were obtained using an FTIR spectrometer (Nicolet Nexus 470, Germany). An atomic force microscope (AFM, Seiko SPI 3800 N, Japan) was used to measure the topographies of the specimens prepared by applying various strains during the coating of the AZO film. XRD measurements were carried out on a Rigaku diffractometer (Rigaku ATX-E, USA) in the 2θ range of 30° to 80° using a CuKα X-ray source. The 2θ scans show the angular positions of ZnO for the PET/AZO specimens. A dual-beam focused ion beam (DB-FIB, FEI Nova-200, USA) was used to prepare the PET/AZO specimens and to investigate the microstructure of the AZO layer that formed on the substrate for various strains. A confocal Raman spectroscope (Renishaw InVia, England) was used to collect spectra related to the Raman bending- and stretching- mode vibrations induced by the neighboring disorder and local geometric disorientation of strained substrates. The spectra were obtained with a 50 mW (514 nm) excitation source and a grating of 1800 gr/mm. The optical properties, including the absorption and transmission spectra, of the PET/AZO specimens were recorded on a spectrophotometer (Jasco V-570, Japan).

3. Results and Discussion

Fig. 3 shows the tensile stress (σ)-strain(ε) curves of the PET substrate obtained at three tensile speeds. The linear $\sigma - \varepsilon$ relationship in the curves can be applied to determine the specimen's elastic modulus. The three curves indicate yielding behavior at a strain of about 4%. Beyond yielding, the nonlinear $\sigma - \varepsilon$ curves can be regressed by the formula $\sigma = \sigma_y[\varepsilon\, E/\sigma_y]^N$ to determine the work hardening index (N) of the PET specimen obtained after applying a strain. Table 3 shows the elastic modulii of three readings for each tensile speed and their mean values. The mean values of the elastic modulii of PET substrates obtained at tensile speeds of 1 mm/min and 10 mm/min exhibit little dependence on the tensile speed. The difference in elastic modulus between these two tensile speeds is quite small. When the tensile speed was increased to 50 mm/min, the mean elastic modulus increased to about 1929 MPa. Table 3 also shows the work hardening indices for the three tensile speeds. The three N values are quite similar. This is due to the N parameter being dependent on the specimen material properties rather than the operating conditions of the tensile test.

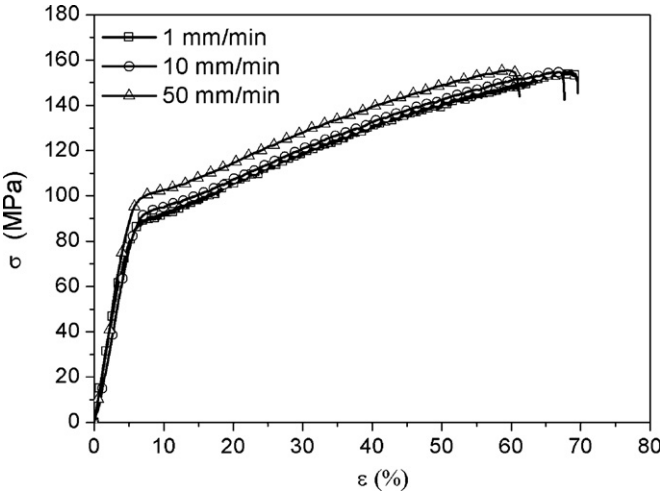

Fig. 3. Results of tensile tests.

In Fig. 4 (a), the infrared absorption spectra of the PET substrates in a wavenumber range of 700 cm^{-1} to 800 cm^{-1} reveal the presence of an absorbance band at about 725 cm^{-1}. This band corresponds to the CH_2 rocking in bending vibrations. From the reflection spectra shown in Fig. 4 (a), an increase in the strain of the PET substrate increases the reflection intensity, which results in a significant decrease in absorption. This figure also demonstrates that the reflection is increased in this wavenumber range if the PET substrate is subjected to bending before the deposition of the thin film, irrespective of the strain applied to the PET substrate. Fig. 4(b) shows absorption at 1410 cm^{-1} for all five specimens. This wavenumber is assigned to the CH_2 and CH_3 deformation created in the bending vibrations. Fig. 4(c) shows the FTIR spectra for the five PET substrates. The intensity spectrum for the PET flat plate (coded by 1) without bending does not show noticeable absorption. However, the spectra for the other four specimens (PET with 0%-6% strain) show an absorption band ranging from 2850 cm^{-1} to 3000 cm^{-1}. This band, with typical infrared absorption frequencies, is associated with stretching vibrations of CH_3 or CH_2 and CH groups.

Table 3
Reslts of tensile tests.

Tensile speed (mm/min)	Yielding stress (MPa)	Strain (%)	Elastic modulus (MPa)	Mean elastic modulus (MPa)	Hardening index (N)	Stardard deviation of N
1	75.100	4.620	1699.095	1595.545	0.254	±0.037
	79.399	4.967	1665.597			
	78.477	5.719	1421.942			
10	76.630	5.508	1443.670	1561.835	0.259	±0.045
	75.347	4.544	1734.507			
	80.205	5.521	1507.329			
50	75.121	3.979	1987.854	1928.773	0.254	±0.054
	76.681	4.215	1909.863			
	82.683	4.578	1888.602			

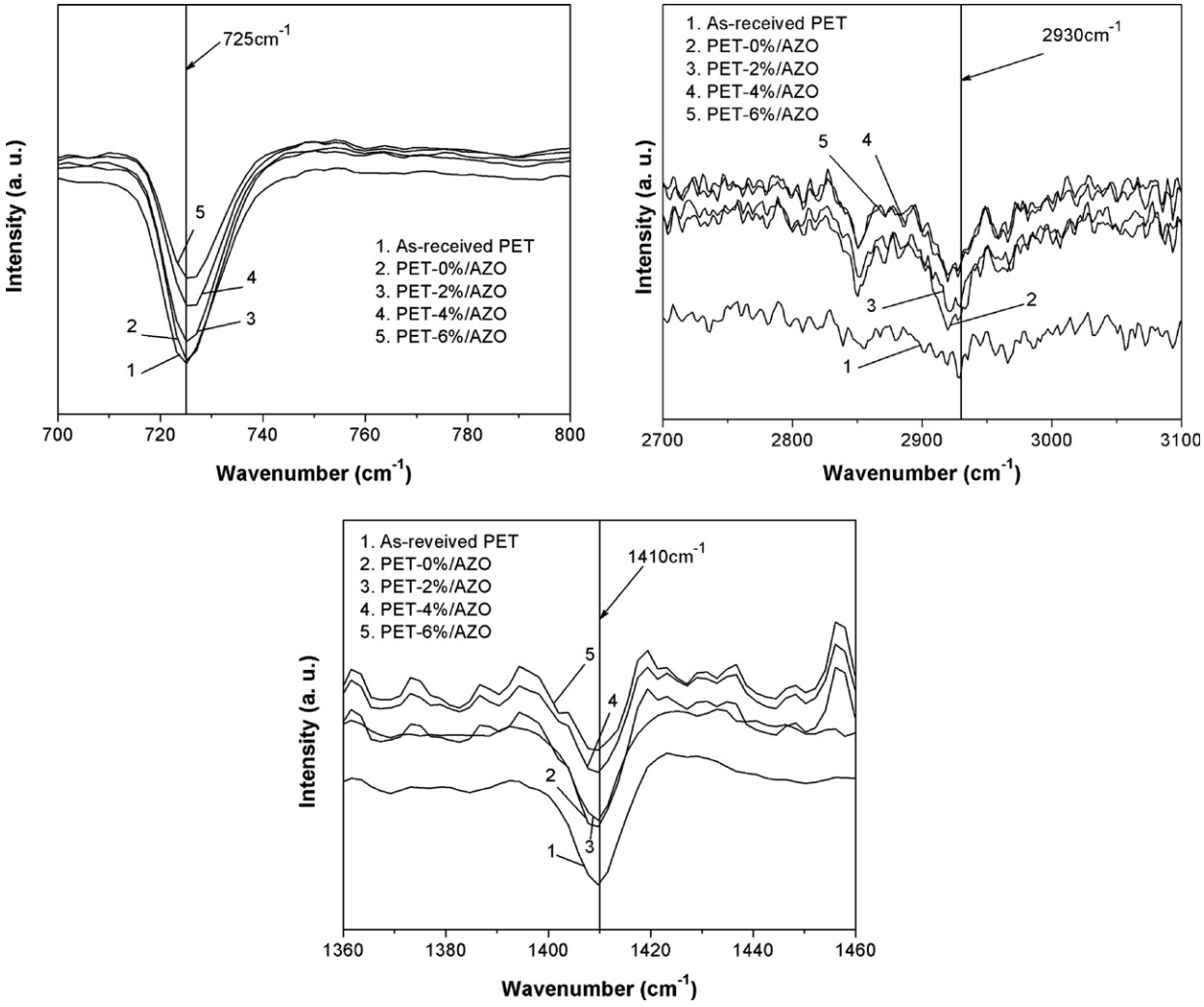

Fig. 4. Experiment data of FTIR-ATR. (a) 700 cm^{-1}–800 cm^{-1}, (b) 1360 cm^{-1}–1460 cm^{-1}, and (c) 2700 cm^{-1}–3100 cm^{-1}.

The strain applied to the PET substrate before coating affects the AZO film thickness and the morphology of PET/AZO specimens. A DB-FIB was used to prepare the lateral surfaces of the specimens with an AZO film. The AZO thicknesses for the PET/AZO specimens are shown in Table 4. The thickness decreased with increasing strain applied to the PET substrate. Fig. 5 shows the topography of the PET flat plate (without bending). Numerous small bulges appear even before the application of strain. Fig. 6(a) to Fig. 6(d) show the topographies of the PET/AZO specimens with strains of 0%, 2%, 4%, and 6%, respectively. Numerous small dome-shaped bulges formed at various densities. The mean surface roughness (Ra) data are shown in Table 4. The mean surface roughness for the specimens initially increased with increasing PET strain, reached a maximum value at a strain of 4%, and then slightly decreased with a further increase in strain.

XRD patterns of the PET/AZO specimens are shown in Fig. 7. The diffraction patterns indicate ZnO film with a strong c-axis (002) orientation along with two weak peaks, ZnO (102) and ZnO (103). This means that the (002) textured film formed in an

Table 4
Experimental results of AZO film for the four coated specimens.

Specimen	Thickness (nm)	Mean Ra (nm)	σ_{film} (MPa)	d-spacing (Å)	Transmittance (%)	Absorption (%)	Band gap (eV)	Mobility (cm^2/V-s)	Carrier concentration (cm^{-3})
PET-0%/AZO	664	15.18	−2.796	2.609	77.36 ± 5.34	0.11 ± 0.03	3.234	0.316	-7.38×10^{19}
PET-2%/AZO	650	16.67	−3.247	2.614	71.43 ± 7.68	0.15 ± 0.05	3.223	0.113	-6.13×10^{19}
PET-4%/AZO	544	22.89	−3.247	2.614	69.12 ± 7.90	0.16 ± 0.05	3.220	0.112	-5.14×10^{19}
PET-6%/AZO	538	20.98	−2.706	2.608	72.29 ± 7.14	0.15 ± 0.05	3.227	0.173	-6.73×10^{19}

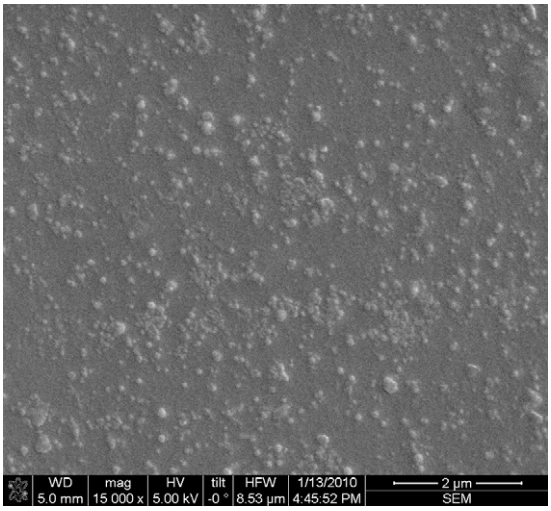

Fig. 5. SEM morphology of as-received PET substrate.

effective equilibrium state, where there is sufficient surface mobility to impinge atoms under certain deposition conditions [10].

Fig. 8 shows the angular peak positions of ZnO (002) evaluated from the XRD 2θ scans for the PET-0%/AZO, PET-2%/AZO, PET-4%/AZO, and PET-6%/AZO specimens. The Bragg diffraction angle of the diffraction peaks of the (002) direction are at a degree of around 34° (2θ) for ZnO films [10]. Diffraction peaks are at 34.35°, 34.28°, 34.28°, and 34.36° for strains of 0%, 2%, 4%, and 6%, respectively. This means that the quality of AZO films initially improved with increasing strain applied to the PET substrate, and then degraded. A homogeneous strain in a film gives rise to a sharp peak with a narrow width in the intensity of the X-ray beam at the Bragg angle [10], as shown in Fig. 7.

The determination of film stress is based on the biaxial strain model. To obtain the film stress σ_{film} parallel to the film surface, the following formula is valid for a hexagonal lattice [22]:

$$\sigma_{\text{film}} = \{[2C_{13}^2 - C_{33}(C_{11} + C_{12})]/2C_{13}\} \times [(C_{\text{film}} - C_{\text{bulk}})/C_{\text{bulk}}] \quad (1)$$

where C_{film}(=5.218, 5.228, 5.228, and 5.216 GPa) and C_{bulk}(=5.2 GPa) are the lattice and strain-free lattice parameters of the film and the strain-free lattice parameter of the ZnO powder sample, respectively. The elastic constants, C_{ij}, for single-crystal ZnO are C_{11} = 209 GPa, C_{12} = 120 GPa, C_{13} = 104 GPa and C_{33} = 214 GPa [23]. The σ_{film} values for

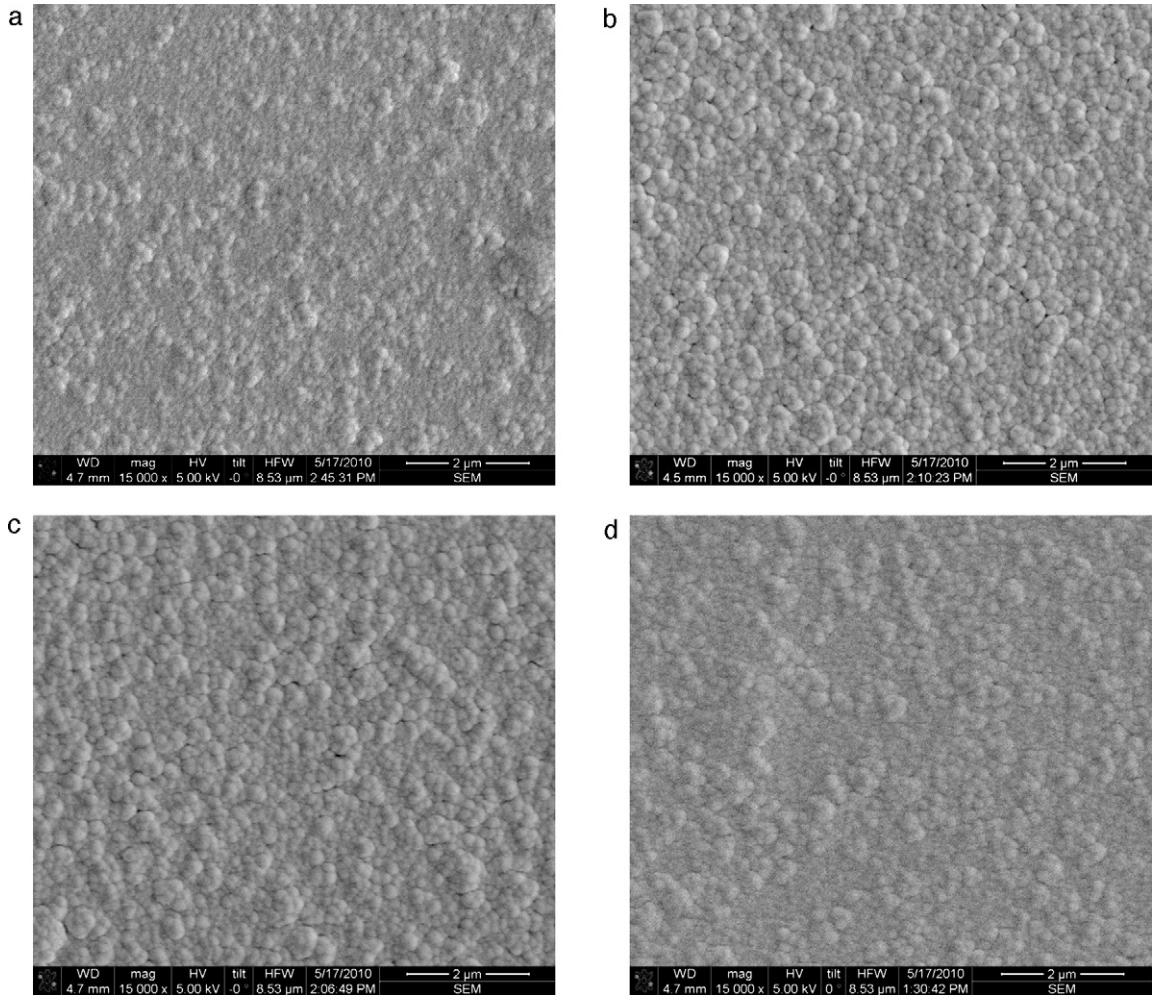

Fig. 6. SEM morphologies of (a) PET-0%/AZO, (b) PET-2%/AZO, (c) PET-4%/AZO, and (d) PET-6%/AZO.

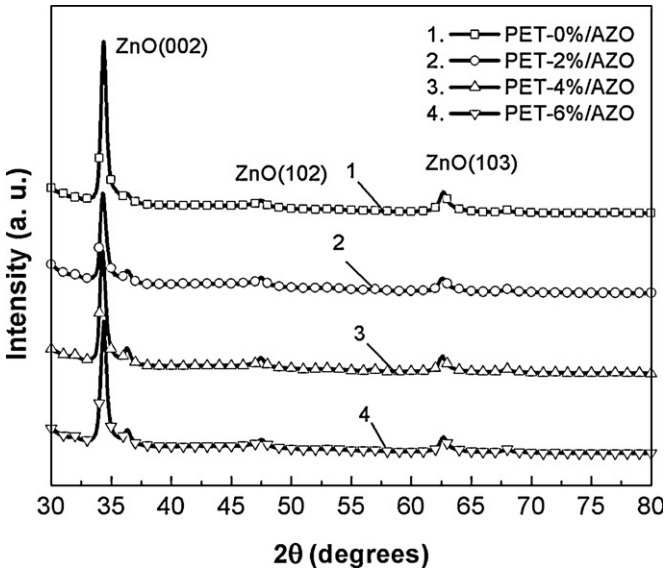

Fig. 7. XRD patterns of the four coated specimens.

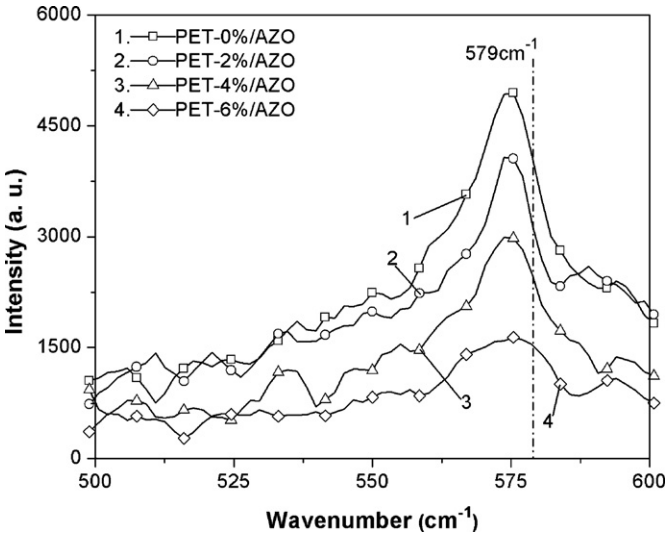

Fig. 9. Raman spectra of the four coated specimens.

these four specimens indicate compressive stresses, as shown in Table 4. The film residual stresses in the PET/AZO specimens for the strains in the substrate are -2.796, -3.247, -3,247, and -2.706 MPa, respectively. Compressive residual stresses are commonly found during the process of sputtering thin films. These biaxial film stresses are likely due to mismatches in the thermal expansion coefficients of the substrate and film after deposition at high temperatures, a combination of film density and crystallographic defects in the thin film structure, and the effects of the bending and strain applied in the PET substrate [10]. Since the film deposition temperature was at 60 °C, the main residual stresses are excluded from the thermal stress [24]. With an increase in the strain applied to the PET substrate, the diffraction peak initially shifted toward 2θ=34° and then moved away from this angle with a further increase in strain (to 6%). Nevertheless, the variance in 2θ due to strain is quite narrow. A large compressive residual stress (with negative sign) was often observed in a specimen with a relatively small 2θ angle. All AZO films formed in the present study show a discrepancy in d-spacing (interplanar spacing) as compared to that for zinc oxide powder. The discrepancy is due to variations of residual stress in the film [25]. The d-spacings are evaluated using the expression, $d = \lambda/(2\sin\theta)$, where the θ angles for the various strains are obtained from the 2θ angles corresponding to the peaks of the XRD patterns shown in Fig. 7, and λ=1.54056 Å for AZO film. Of note, the change in d-spacing due to two different strains being applied to the substrate was linearly proportional to the difference in the σ_{film} values corresponding to these two strains.

Fig. 9 shows the Raman spectra for the PET substrates. Based on an earlier report [14], the results in this figure are expected to be A_1-LO modes [26]. The highest intensity of the standard A_1-LO mode is at 579 cm^{-1}. The shifting in band position with respect to this highest intensity can be attributed to several factors, including residual stress, structural disorder, and crystal defect in the films and the presence of dopants. Residual stress is the governing factor. Fig. 10 shows the

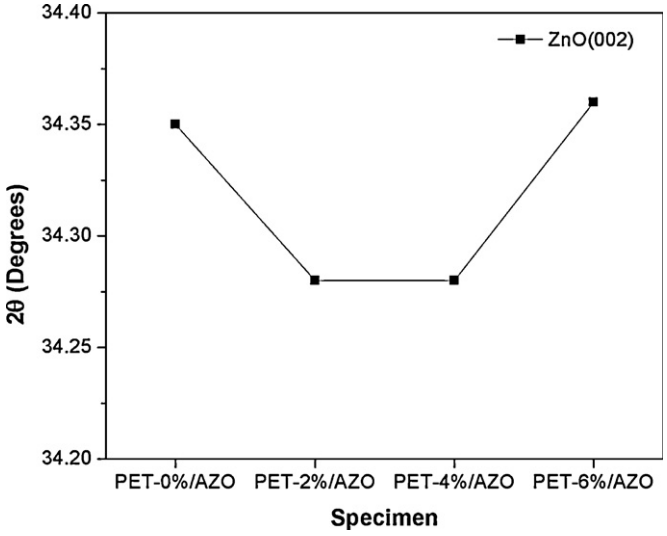

Fig. 8. Blue-shift of XRD pattern peaks.

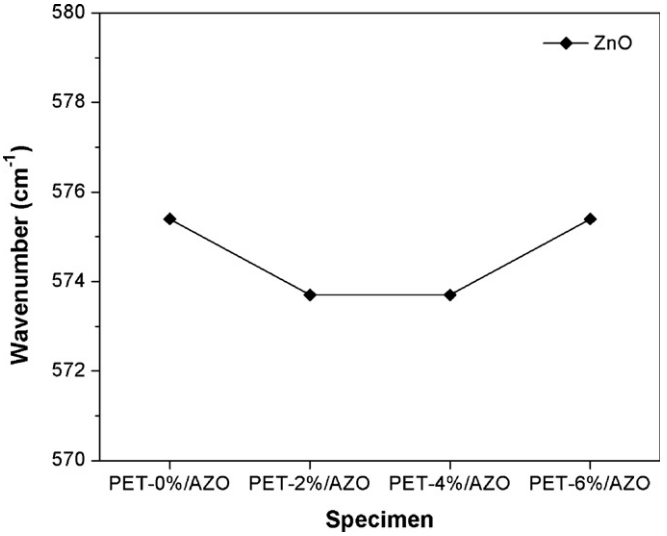

Fig. 10. Blue-shift of Raman spectra peaks.

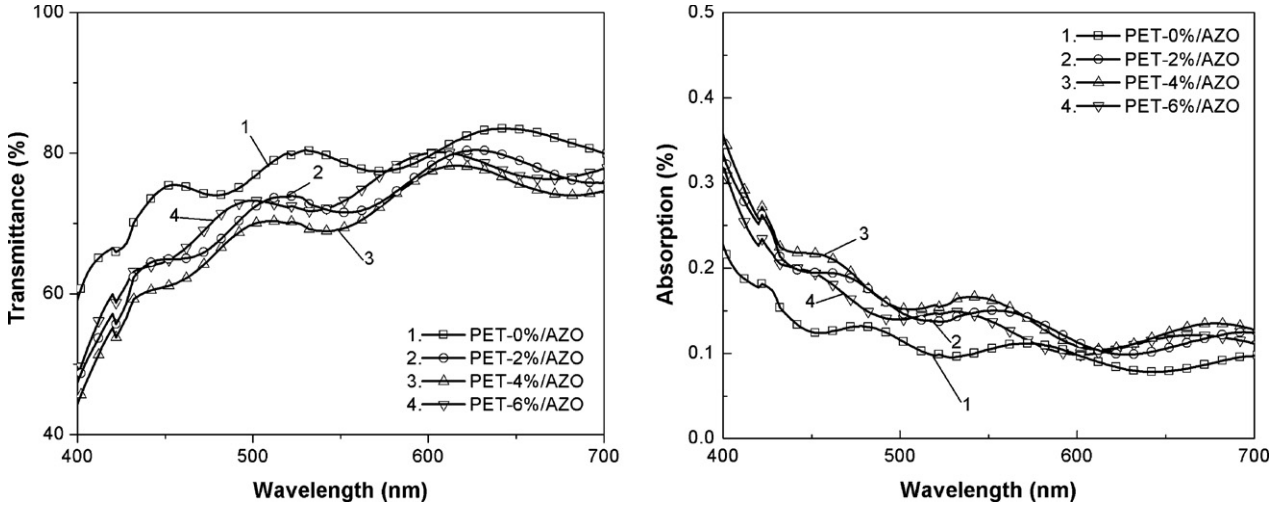

Fig. 11. (a) Transmittance and (b) absorption data as functions of wavelength.

wavenumbers of the highest intensities for the four specimens. The wavenumber (unit: cm^{-1}) behavior demonstrated in the Raman blue-shift is inversely proportional to that demonstrated in d-spacing (see Table 4). Regarding shape difference in the Raman spectra, an increase in the strain applied to the PET substrate led to neighboring disorder and local geometric disorientation, affecting the Raman bending- and stretching-mode vibrations as suggested by the molecular theory of vibration. The Raman bands became broader with increased strain applied to the PET substrate. Zhang *et al.* [27] found that a decrease in the crystallite dimension to the nanometer scale causes a frequency shift and a broadening of Raman bands as a result of phonon confinement.

The optical transmittance spectra of AZO thin films deposited on PET substrates with various strains are shown in Fig. 11(a). The films are highly transparent in the visible range. An increase in the substrate strain reduces the transmittance of the PET/AZO specimen in the light wavelength range of 400 nm to 700 nm. Fig. 11 (b) shows the absorption spectra for the four specimens. For all four curves, the absorption decreases with increasing light wavelength. A specimen with a high transmittance thus has low absorption. The mean values of the transmittance and absorption for the four PET/AZO specimens are shown in Table 4. Of the four specimens, the PET-0%/AZO specimen has the highest transmittance and the lowest absorption, whereas the PET-4%/AZO specimen has the lowest transmittance and the highest absorption. The absorption coefficient (α) can be calculated using [28]:

$$\alpha = \ln(1/T)/d \tag{2}$$

where T denotes transmittance and d denotes film thickness. The optical band gap, Eg, dependent on the absorption coefficient, α, can be written as [29]:

$$(\alpha h\nu)^2 = A(h\nu - Eg) \tag{3}$$

where A is a constant. Eg can be determined by extrapolating the linear portion of the curve to intersect the $h\nu$ axis. Fig. 12 shows the variations of α^2 with photon energy. The Eg values obtained from extrapolations for the four PET/AZO specimens are also shown in Fig. 12. The figure shows the sequence:$(Eg)_{0\%} > (Eg)_{6\%} > (Eg)_{2\%} > (Eg)_{4\%}$. This sequence indicates that an increase in the optical band gap is disadvantageous for lowering the mean absorption, but is advantageous for increasing the mean transmittance of specimens. The trend in the optical band gap due to a change in the strain applied to the substrate is the same as that for transmittance.

Four-point sheet resistances (R) of the four specimens were measured; the results are shown in Fig. 13. The experimental data of R show the sequence:$(R)_{4\%} > (R)_{2\%} > (R)_{6\%} > (R)_{0\%}$. Of note, the sequence for the sheet resistances is opposite to those shown for the optical band gap (Eg) and transmittance.

Table 4 shows the experimental data of the optical band gap (Eg), carrier mobility, and carrier concentration for the PET/AZO specimens. The optical band gaps and carrier mobilities

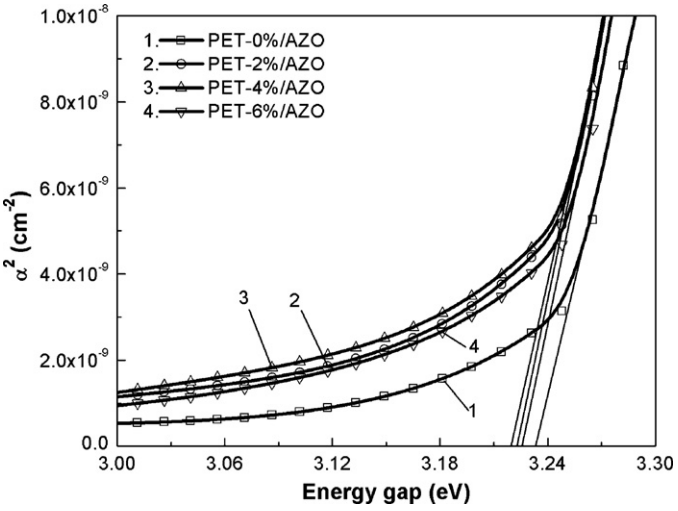

Fig. 12. Band gap energy of the four coated specimens.

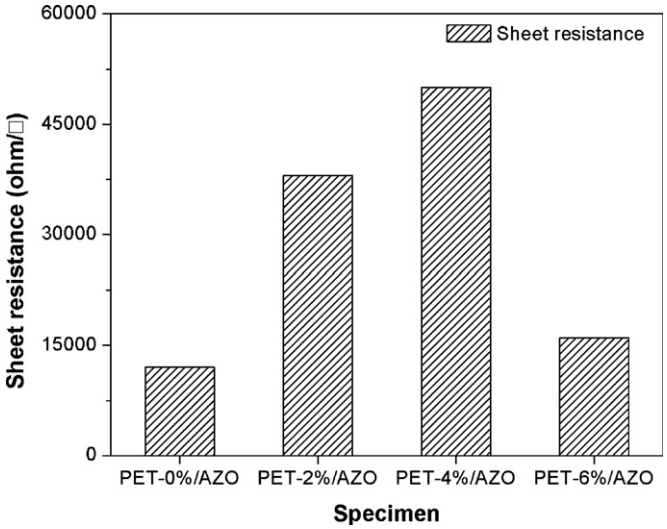

Fig. 13. Four-point sheet resistances of the four coated specimens.

and concentrations for the four specimens exhibit the same sequence in terms of magnitude. This is consistent with Eq. (2) and Eq. (3). However, the trend for the four sheet resistances is exactly opposite to that for carrier mobility. A high carrier mobility is thus obtained for a specimen with a relatively low sheet resistance. It can thus be concluded that a higher compressive stress in the AZO film results in a lower optical band gap and a lower transmittance; it also led to an increase in the sheet resistance of the AZO film, and thus a lower carrier mobility, and carrier concentration.

4. Conclusions

The elastic modulus of the PET substrate is only slightly dependent on the tensile speed below a certain speed. The elastic modulus increases with increasing tensile speed. The work hardening index of PET is independent of the tensile speed. An increase of strain in the PET substrate generally enhances the intensities of the absorbance peaks situated at about 725 cm^{-1}, 1410 cm^{-1}, and 2850-3000 cm^{-1}. These peaks are related to the bending and stretching vibrations of CH, CH_2 and CH_3 groups. The AZO film thickness decreased with increasing strain applied into the PET substrate. The topographies of the PET/AZO specimens were affected by the strain in the substrate. The maximum surface roughness was obtained for the specimen with a strain of 4%. The diffraction peaks of XRD patterns show ZnO (002) to be dominant in the AZO films. The quality of AZO film initially improved with increasing strain, and then degraded. Compressive residual stresses formed in the specimens. The residual stress increased with decreasing XRD 2θ angle. The change in d-spacing due to two different strains applied to the substrate is linearly proportional to the change in the residual stress σ_{film} corresponding to the two strains. A higher compressive stress in the AZO film resulted in a lower optical band gap and a lower transmittance; it also led to an increase in the sheet resistance of the AZO film, and thus a lower carrier mobility and carrier concentration. The extreme values of the parameters were obtained for the specimen with a strain of 4%.

References

[1] P. Yuan, C.S.P. Sung, Angular characterization of polymer surfaces by FTIR ATR dichroism with a rotatable truncated hemispheric crystal, Macromolecules 24 (1991) 6095–6103.
[2] S.M. Liu, F.Q. Liu, H.Q. Guo, Z.H. Zhang, Z.G. Wang, Correlated structural and optical investigation of terbium-doped zinc oxide nanocrystals, Phys. Lett. A 271 (2000) 128–133.
[3] C.J.M. van den Heuvel, H.M. Heuvel, W.A. Fassen, J. Veurink, L.J. Lucas, Molecular changes of PET yarns during stretching measured with rheo-optical infrared spectroscopy and other techniques, J. Appl. Polym. Sci. 49 (1993) 925–934.
[4] E.M. Bachari, S. Ben Amor, G. Baud, M. Jacquet, Photoprotective zinc oxide coatings on polyethylene terephthalate films, Mater. Sci. Eng. B 79 (2001) 165–174.
[5] L. Wu, Y. Wu, X. Pan, F. Kong, Synthesis of ZnO nanorod and the annealing effect on its photoluminescence property, Opt. Mater. 28 (2006) 418–422.
[6] J. Tao, X. Dong, T. Wang, Y.H. Cui, Crystallization behaviour of nano-ZnO/PET and nano-ZnO/polyethylene glycol (PEG)/PET composites by in situ polymerization, Key Engineering Materials 334–335 (2007) 853–856.
[7] M. Tzolov, N. Tzenov, D. Dimova-Malinovska, M. Kalitzova, C. Pizzuto, G. Vitali, G. Zollo, I. Ivanov, Vibrational properties and structure of undoped and Al-doped ZnO films deposited by RF magnetron sputtering, Thin Solid Films 379 (2000) 28–36.
[8] W. Water, S.Y. Chu, Physical and structural properties of ZnO sputtered films, Mater. Lett. 55 (2002) 67–72.
[9] K. Matsubara, H. Tampo, H. Shibata, A. Yamada, P. Fons, K. Iwata, S. Niki, Band-gap modified Al-doped Zn1 − xMgxO transparent conducting films deposited by pulsed laser deposition, Appl. Phys. Lett. 85 (2004) 1374–1376.
[10] R. Hong, J. Shao, H. He, Z. Fan, Influence of buffer layer thickness on the structure and optical properties of ZnO thin films, Appl. Surf. Sci. 252 (2006) 2888–2893.
[11] S.M. Park, T. Ikegami, K. Ebihara, P.K. Shin, Structure and properties of transparent conductive doped ZnO films by pulsed laser deposition, Appl. Surf. Sci. 253 (2006) 1522–1527.
[12] T. Makino, K. Tamura, C.H. Chia, Y. Segawa, M. Kawasaki, A. Ohtomo, H. Koinuma, Optical properties of ZnO:Al epilayers: Observation of room-temperature many-body absorption-edge singularity, Phys. Rev. B 65 (2002) 4, 121201-1.
[13] R.K. Gupta, K. Ghosh, R. Patel, S.R. Mishra, P.K. Kahol, Band gap engineering of ZnO thin films by In2O3 incorporation, J. Cryst. Growth 310 (2008) 3019–3023.
[14] R. Vinodkumar, I. Navas, S.R. Chalana, K.G. Gopchandran, V. Ganesan, R. Philip, S.K. Sudheer, V.P. Mahadevan Pillai, Highly conductive and transparent laser ablated nanostructured Al: ZnO thin films, Appl. Surf. Sci. 257 (2010) 708–716.
[15] J.J. Ding, H.X. Chen, S.Y. Ma, The Al-doping and post-annealing treatment effects on the structural and optical properties of ZnO:Al thin films deposited on Si substrate, Appl. Surf. Sci. 256 (2010) p.4304–4309.
[16] B.G. Kim, J.Y. Kim, S.J. Lee, J.H. Park, D.G. Lim, M.G. Park, Structural, electrical and optical properties of Ga-doped ZnO films on PET substrate, Appl. Surf. Sci. 257 (2010) 1063–1067.
[17] E. Fortunato, P. Nunos, A. Marques, D. Costa, H. Águas, I. Ferreira, M.E.V. Costa, M.H. Godinho, P.L. Almeida, J.P. Borges, R. Martins, Transparent, conductive ZnO:Al thin film deposited on polymer substrates by RF magnetron sputtering, Surf, Coat. Technol. 151–152 (2002) 247–251.
[18] A.N. Banerjee, C.K. Ghosh, K.K. Chattopadhyay, H. Minoura, A.K. Sarkar, A. Akiba, A. Kamiya, T. Endo, Low-temperature deposition of ZnO thin films on PET and glass substrates by DC-sputtering technique, Thin Solid Films 496 (2006) 112–116.

[19] D. Song, Effects of rf power on surface-morphological, structural and electrical properties of aluminium-doped zinc oxide films by magnetron sputtering, Appl. Surf. Sci. 254 (2008) 4171–4178.
[20] K.A. Sierros, D.A. Banerjee, N.J. Morris, D.R. Cairns, I. Kortidis, G. Kiriakidis, Mechanical properties of ZnO thin films deposited on polyester substrates used in flexible device applications, Thin Solid Films 519 (2010) 325–330.
[21] D.J. Kwak, J.H. Kim, B.W. Park, Y.M. Sung, M.W. Park, Y.B. Choo, Growth of ZnO:Al transparent conducting layer on polymer substrate for flexible film typed dye-sensitized solar cell, Curr. Appl. Phys. 10 (2010) 282–285.
[22] A. Segmuller, M. Murakami, X-Ray diffraction analysis of strains and stresses in thin films, Analytical techniques for thin films, Academic Press, Boston, 1988, 143-200.
[23] R. Cebulla, R. Wendt, K. Ellmer, Al-doped zinc oxide films deposited by simultaneous rf and dc excitation of a magnetron plasma: Relationships between plasma parameters and structural and electrical film properties, J. Appl. Phys. 83 (1998) 1087–1095.
[24] B. Window, K.H. Muller, Strain, ion bombardment and energetic neutrals in magnetron sputtering, Thin Solid Films 171 (1989) 183–196.
[25] T.J Vink, W. Walrave, J. L.C. Daams, P.C. Baarslag, J.E.A.M. van der Meerakker, On the homogeneity of sputter-deposited ITO films Part I. Stress and microstructure, Thin Solid Films 266 (1995) 145–151.
[26] U.Ya. Ozgur, I. Alivov, C. Liu, A. Teke, M.A. Reshchikov, S. Dogan, V. Avrutin, S.-J. Cho, H. Morkoc, A comprehensive review of ZnO materials and devices, J. Appl. Phys. 98 (2005) 041301 (103 pages).
[27] W.F. Zhang, Y.L. He, M.S. Zhang, Z. Yin, Q. Chen, Raman scattering study on anatase TiO_2 nanocrystals, J. Phys. D: Appl. Phys. 33 (2000) 912–916.
[28] W. Miao, X. Li, Q. Zhang, L. Huang, Z. Zhang, L. Zhang, X. Yan, Transparent conductive In_2O_3:Mo thin films prepared by reactive direct current magnetron sputtering at room temperature, Thin Solid Films 500 (2006) 70–73.
[29] V.R. Shinde, T.P. Gujar, C.D. Lokhande, R.S. Mane, S.H. Han, Mn doped and undoped ZnO films: A comparative structural, optical and electrical properties study, Mater, Chem. Phys. 96 (2006) 326–330.